ACS Catalysis

pubs.acs.org/acscatalysis
Research Article

Metallic Pd–Cu Alloy Phases Drive Selective Heterogeneous Electrochemical Ketonization of 1-Butene

Chenyu Jiang, Benjamin Moss, Alexis Lindenfelser, Jung Tae Kim, Yuzhang Li, and Karthish Manthiram*

Cite This: ACS Catal. 2026, 16, 7429–7438
Read Online

ACCESS | Metrics & More | Article Recommendations | Supporting Information

ABSTRACT: Electrification of 2-butanone synthesis via ketonization of 1-butene offers a viable pathway to reduce emissions associated with its production as a commodity chemical and enhance its prospects as a clean carbon-based synthetic fuel. However, the direct electrochemical ketonization of alkenes remains underexplored, with previous studies largely limited to epoxides and glycols. Herein, we report an electrochemical heterogeneous system optimized for 1-butene ketonization, converting 1-butene to 2-butanone using a bimetallic PdCu catalyst in aqueous electrolytes. The system achieves a Faradaic efficiency of 20% and a partial current density of 0.6 mA/cm^2 at 1.8 V_{RHE}. In comparison to monometallic Pd and oxidized PdCu analogs, the PdCu catalyst doubles the ketonization Faradaic efficiency and quadruples the production rate. Postelectrolysis characterization reveals that PdCu preserves the surface metallic alloy phase under anodic polarization, which likely accounts for the enhanced ketonization activity. This work demonstrates the significance of the Pd–Cu speciation dynamics and provides a framework for designing selective electrocatalysts for alkene ketonization.

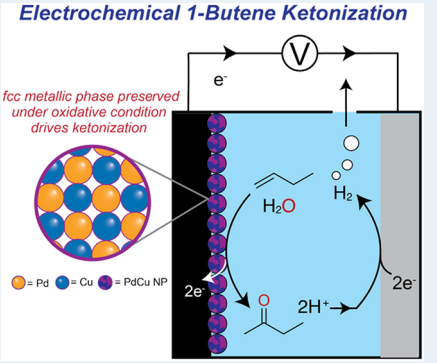

KEYWORDS: *electrocatalysis, electrochemical 1-butene oxidation, methyl ethyl ketone, ketonization, catalyst characterization, heterogeneous catalysis*

INTRODUCTION

Electrifying the chemical industry and transportation sector is a step toward achieving carbon neutrality and reducing reliance on fossil fuels, as electricity from renewable sources is becoming increasingly available and decreasing in cost.[1] Rather than relying on elevated temperatures and pressures, electrochemistry employs applied voltage to drive chemical reactions, offering a more sustainable alternative to commodity chemical production. Therefore, electrochemical technologies have emerged as a promising strategy for generating clean carbon-based synthetic fuels compatible with existing energy infrastructure.[2] One potential target for electrochemical synthesis is 2-butanone. In addition to its commercial value (~$4 billion global market size[3]), 2-butanone is a promising synthetic fuel candidate for spark-ignition engines due to its high knock resistance and gasoline-like enthalpy of vaporization.[4] Industrial production of 2-butanone is commonly achieved via a high-temperature hydration of butylene in concentrated acids, an energy-intensive process.[5] Electrification could, in principle, reduce the emissions associated with 2-butanone production, enhancing its viability as a sustainable synthetic fuel.

A particularly attractive pathway to electrify 2-butanone production is through the electro-oxidation of 1-butene. Direct alkene electro-oxidation, achieved by means of water activation over heterogeneous electrocatalysts at ambient conditions, has garnered considerable attention.[6] This electrochemical approach not only replaces the energy-intensive conditions of traditional thermochemical methods but also utilizes water as the oxygen-atom source without the need for stronger, explosive oxidants, such as hydrogen peroxide.[7−17] However, selective ketonization in alkene electro-oxidation remains significantly underdeveloped in comparison to other processes like epoxidation. Moreover, propylene oxidation has been the primary focus owing to the high industrial value of propylene oxide and propylene glycol. While ketones are observed particularly with Pd-based electrocatalysts,[11−14] this reactivity has been frequently attributed to homogeneous reactions catalyzed by dissolved Pd species from catalyst corrosion rather than true heterogeneous catalysis.[12,13] Additionally, more selective epoxidation electrocatalysts, such as Pd–Pt alloys, have been observed to largely suppress ketonization.[9] While theoretical and empirical investigations have revealed possible potential-dependent selectivity in electrochemical oxidation of alkenes,[11,15] suggesting that the ketone selectivity can be tuned through rational catalyst design and external voltage control, heterogeneous electrocatalytic systems specifically focused on selective alkene ketonization have yet to be report.

Received: December 15, 2025
Revised: March 17, 2026
Accepted: March 17, 2026
Published: March 31, 2026

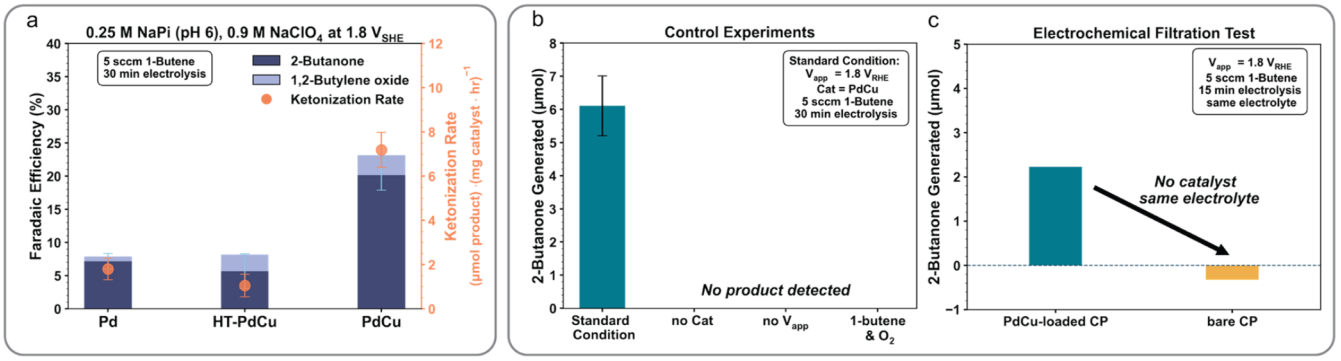

Figure 1. Electrochemical oxidation of 1-butene over Pd, PdCu, and HT-PdCu (heat-treated preoxidized PdCu). (a) Faradaic efficiency and ketone production rate for direct electrochemical 1-butene ketonization with Pd-based and Cu-based catalysts in aqueous electrolytes. Control experiments on PdCu (b) and the electrochemical filtration test (c) used to confirm the electrochemical and heterogeneous nature of the catalysis. In panel (c), the standard experiment is interrupted and bare carbon paper (CP) loaded in place of PdCu-loaded CP and the experiment continued. The negative value with bare CP may arise from product loss from transferring the electrolyte out of and back to the electrochemical cell. Error bars represent standard deviations from the mean of multiple replicates ($n \geq 2$) using fresh electrodes for each measurement. Applied potential was 100% *iR* compensated.

By contrast, several nonelectrochemical routes for converting alkenes to ketones are known. Wacker-Tsuji oxidation, a well-studied homogeneous alkene ketonization reaction, employs a $PdCl_2$ catalyst with a $CuCl_2$ cocatalyst.[18,19] Similarly, Pd−Cu immobilized on zeolites has been demonstrated for thermal heterogeneous catalysis.[20−22] Building on these precedents, we sought to explore electrochemical alkene ketonization by heterogeneous Pd−Cu alloys in aqueous electrolytes.[23−27] We selected 1-butene as the substrate and 2-butanone as the target product owing to its industrial relevance and potential application as a synthetic fuel. The aqueous electrochemical oxidation of 1-butene is inherently more challenging than that of propylene, as a longer carbon chain results in lower solubility in water, limiting 1-butene availability at the electrode surface. Furthermore, increased carbon chain of alkene is associated with reduced reactivity in heterogeneous catalysis.[28−31] Propylene epoxidation is more difficult than ethylene epoxidation due to the activated allylic C−H group, which makes side reactions yielding acrolein and allyl alcohol more facile.[29−31] By extension, 1-butene electro-oxidation presents even greater challenges regarding both reactivity and selectivity.

Herein, we present a catalytic system optimized for heterogeneous ketonization of 1-butene by using an electrocatalyst derived from a bimetallic PdCu alloy. Under electrochemical conditions, Cu-based catalysts are known to undergo dynamic surface reconstruction, which is challenging to predict due to local electric field effects and pH swings at the electrode−electrolyte interface.[32−34] Such surface evolution can present both beneficial and detrimental influences on catalytic performance, leading to either enhanced activity or deactivation.[35−37] We therefore characterized the catalysts in both their pristine state and after bulk electrolysis with 1-butene to gain insights into the effects of catalyst evolution on ketonization and to inform future catalyst design.

RESULTS AND DISCUSSION

Establishing the PdCu Catalyst and Heterogeneous Electrochemical 1-Butene Ketonization

As previous studies on alkene electro-oxidation indicate that ketonization is likely favored with metallic catalysts,[11,12] we prepared a PdCu catalyst via coreduction of $PdCl_2$ and $CuCl_2$ with ascorbic acid at 10 °C following a literature procedure.[24] The monometallic Pd analogue was prepared using the same method with $PdCl_2$ as the sole precursor to isolate the effects of alloying. While metallic Pd favors ketonization in electrochemical alkene oxidation, Pd(II) has been proposed as the catalytically active species in heterogenized thermochemical Wacker-Tsuji oxidation.[18,19] Thus, we also prepared a preoxidized sample of PdCu, which we refer to as HT-PdCu, by annealing PdCu in static air at 400 °C for 3 h. Catalyst-loaded carbon paper electrodes were fabricated by drop-casting the catalyst ink and subsequently coated with Nafion.[9] Electrochemical experiments were conducted using the same home-built, three-electrode gas-diffusion cell operated in a flow-through configuration, identical to that used in our previous study.[9] Details of the synthetic procedure, electrode fabrication, and electrochemical study are provided in the Supporting Information.

Catalytic performance was evaluated by chronoamperometry at 1.8 V_{RHE} in a pH 6 electrolyte (0.25 M sodium phosphate (NaPi) and 0.9 M $NaClO_4$) under an ambient flow of 1-butene. Products were quantified with ^1H nuclear magnetic resonance (NMR) spectroscopy using sodium trimethylsilylpropanesulfonate as the internal standard. The monometallic Pd catalyst showed poor performance, achieving less than 10% Faradaic efficiency (FE) for 2-butanone, and the preoxidized sample, HT-PdCu, intended to replicate oxidation states effective for thermochemical Wacker-Tsuji oxidation, demonstrated similarly low FE. Interestingly, relative to Pd and HT-PdCu, PdCu achieved twice the FE and a 4-fold increase in the production rate for 2-butanone (Figure 1a). Furthermore, the less oxidized catalysts, Pd and PdCu, displayed substantially higher selectivity toward 2-butanone, with ketone-to-epoxide ratios of 6:1 and 5:1, respectively, compared to 2:1 for HT-PdCu. The improved ketone selectivity indicates the significance of the less oxidized catalyst surface in ketonization, as proposed in previous studies,[11,14] and hints at a reaction pathway distinct from the thermochemical route driven by high valent Pd(II). The pronounced enhancement in ketonization activity of PdCu in comparison to that of Pd further suggests that mixing Pd−Cu is likely to play a key role in facilitating the observed ketonization reactivity.

https://doi.org/10.1021/acscatal.5c08675
ACS Catal. 2026, 16, 7429−7438

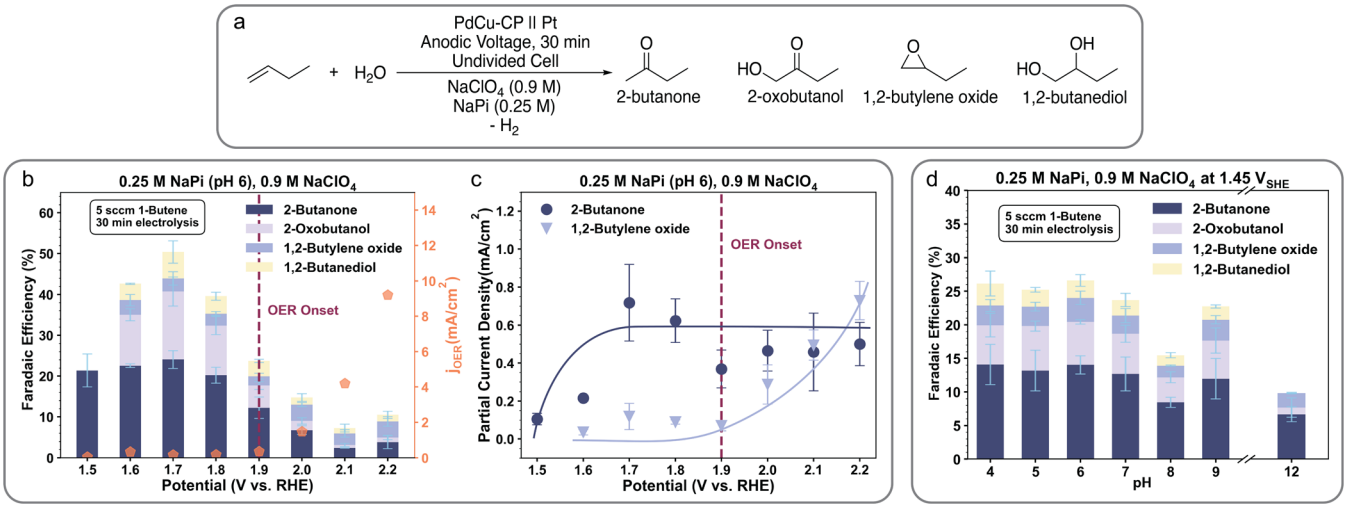

Figure 2. Potential- and pH-dependence of electrochemical oxidation of 1-butene by PdCu. (a) Reaction scheme showing the major organic products in 1-butene oxidation observed. Potential dependence of the FEs of PdCu (b) and the partial current densities (c) for 2-butanone and 1,2-butylene oxide. The solid lines are guides for the eye. (d) Dependence of the FE of the PdCu catalysts on pH. Potentials in this figure were 100% *iR* corrected. Error bars represent standard deviations calculated from the mean of multiple replicates ($n \geq 3$) with fresh electrodes for each measurement. Applied potentials were 100% *iR* compensated.

Since $PdCl_2$ and $CuCl_2$ are known to cocatalyze alkene oxidation under molecular oxygen (O_2) in the homogeneous Wacker-Tsuji pathway,[18] one might attribute the observed ketonization in the PdCu electrocatalytic system to non-electrochemical or homogeneous reactions arising from dissolved Pd species in the electrolyte, as suggested in previous studies.[12,13] To interrogate the nature of 1-butene oxidation in this system, we conducted a series of control experiments (Figure 1b,c). We verified that 1-butene oxidation by PdCu occurs through an electrochemical rather than a thermochemical pathway, given that no products were detected in the absence of an anodic potential (Figure 1b). Because O_2 acts as the oxidant in the Wacker-Tsuji oxidation and can be generated *in situ* under operating conditions, particularly at higher potentials, it is plausible that O_2-mediated thermal oxidation could contribute to the observed ketone formation. However, when a mixed 1-butene/O_2 stream ($P_{1-\text{butene}} = P_{O_2} = 0.5$) was introduced without applying the anodic potential, no products were detected, thereby excluding the thermal O_2-mediated pathway. Inductively coupled plasma (ICP) analysis showed minimal leaching of Pd and Cu into the post-electrolysis electrolyte (0.2 ppm and 6.5 ppb, respectively). To further rule out the contributions from any dissolved species, we conducted an electrochemical "filtration test" following our previous protocol (Figure 1c).[38] Halfway through electrolysis, the catalyst-loaded carbon paper was replaced with bare carbon paper. The same electrolyte was reused, and electrolysis was then resumed. No additional products were detected after swapping the catalyst-loaded carbon paper, consistent with the control experiment in the absence of the catalyst (Figure 1b). Collectively, these results corroborate that the observed 1-butene oxidation reactivity originates exclusively from a heterogeneous electrochemical process on the PdCu surface.

Role of Potential and pH

Having established the efficiency and heterogeneous nature of 1-butene ketonization in the PdCu electrocatalytic system, we next examined the effects of the applied potential and electrolyte pH. Considering the possible evolution of the catalyst surface during anodic polarization, a freshly prepared catalyst-loaded carbon paper was used for each electrolysis experiment to eliminate any influence from the sample history. Electro-oxidation of 1-butene with PdCu generates several organic products with 2-butanone, 2-oxobutanol, 1,2-butylene oxide, and 1,2-butanediol as the major products (Figure 2a). Products were identified using ^{1}H NMR (see Figure S3 for NMR assignment). Figure 2b shows the potential-dependent product selectivity at pH 6, alongside the oxygen evolution reaction (OER) current density obtained via chronoamperometry in the absence of 1-butene. OER was especially evident at potentials more anodic than 1.9 V_{RHE}. The partial current density toward each product at each potential is provided in the SI (Figure S4).

Until 1.8 V_{RHE}, the FE for 2-butanone remains nearly constant at ~20%, then decreases above 1.9 V_{RHE}, coinciding with the onset of the OER current. 2-Oxobutanol follows a similar trend with an FE of approximately 10% prior to the onset of the OER. We note that 2-butanone was the only detectable product at 1.5 V_{RHE}, indicating that the formation of the other products requires a higher overpotential. Above 1.9 V_{RHE}, the epoxidation activity leading to 1,2-butylene oxide surpasses ketonization, and its partial current density closely trends with the OER current. One possible source of 2-oxobutanol is the overoxidation of 1,2-butanediol. However, the ratio of 2-oxobutanol to 1,2-butanediol decreases with more oxidizing potentials, inconsistent with the overoxidation hypothesis (Figure S7a). As both the FE and partial current density for 2-oxobutanol exhibit a similar trend as 2-butanone (Figures 2b and S4), we speculate that 2-oxobutanol is likely formed through a related reaction pathway as 2-butanone.

Given the involvement of multiple reaction pathways and the participation of either *OH/OH^- or H^+ species, we investigated the pH-dependence of the reaction. The pH of the electrolyte has little impact on either ketonization or epoxidation between pH 4—7 and at pH 9 under 1.45 V_{SHE}, while pH 8 and 12 result in diminished overall product generation (Figure 2d). In contrast to previous observations of a Pd−Pt alloy catalyst optimized for propylene epoxidation,

https://doi.org/10.1021/acscatal.5c08675
ACS Catal. 2026, 16, 7429−7438

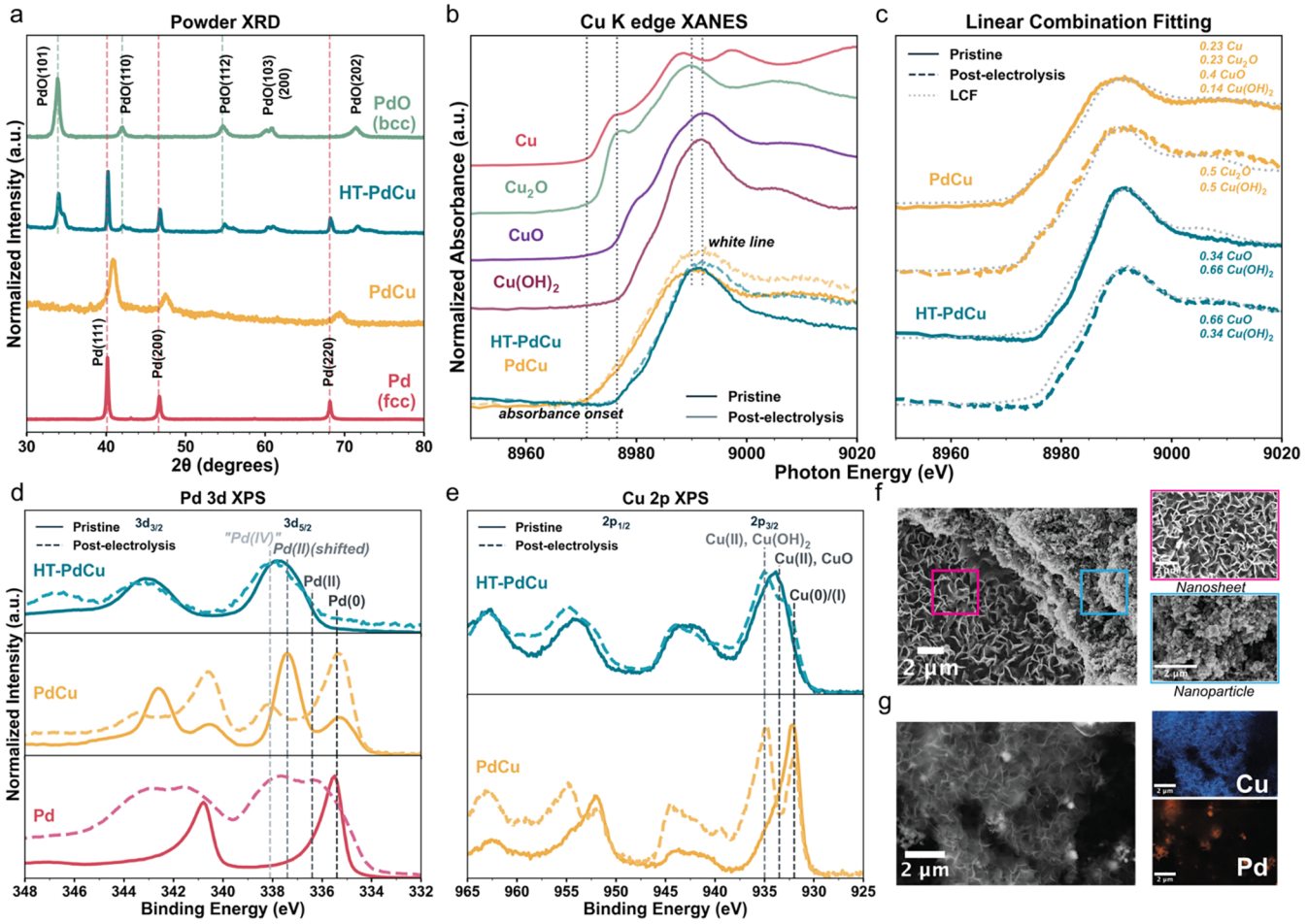

Figure 3. Characterization of Pd, PdCu, and HT-PdCu. (a) XRD patterns. fcc: face-centered cubic; bcc: body-centered cubic. (b) Normalized XANES data, shown *ex situ* spectra for pristine and postelectrolysis PdCu and HT-PdCu as well as standard Cu materials. (c) Linear combination fitting (LCF) for PdCu and HT-PdCu using the spectra of Cu standard materials. Alternative fittings are provided in SI Section D.4. (d, e) Normalized Pd 3d and Cu 2p XPS spectra of Pd, PdCu, and HT-PdCu in the pristine and postelectrolysis state. (f) Two types of surface morphologies observed in the postelectrolysis PdCu. (g) Nanosheet morphology in postelectrolysis HT-PdCu and the EDS spectra of Cu and Pd.

where a higher amount of propylene glycol is detected at more acidic pHs due to more facile acid-catalyzed hydrolysis,[9] the PdCu system at 1.45 V_{SHE} does not show an apparent selectivity toward 1,2-butanediol under acidic conditions (Figure S7d). Additionally, no 1,2-butanediol was detected at pH 12. The lack of correlation between 1,2-butanediol and 1,2-butylene oxide suggests that 1,2-butanediol was not generated through epoxide ring opening but more likely through a direct glycol pathway due to allylic activation.[12,13]

Our potential-dependence data show that ketonization is favored at lower potentials, consistent with previous Pd-based propylene electro-oxidation studies.[11−13] Ketonization on PdCu exhibits a potential dependence with a Tafel slope of 131 ± 38 mV/dec (Figure S5) that attenuates at more oxidizing potentials within the OER regime (Figure 2c). This behavior contrasts sharply with that of epoxidation, which shows the opposite trend with potential independence below the OER onset potential and a stronger potential dependence in the OER regime (Tafel slope = 96 ± 25 mV/dec, Figure S5). The saturation behavior of ketonization is unlikely to arise from mass-transport limitations, as supported by theoretical mass-transport analysis (SI Section D.2.). The weak dependence of partial current densities on both potential and pH suggests that ketonization with PdCu is likely to be limited by a thermochemical step, such as the oxygen-atom transfer to 1-butene or hydrogen-atom migration leading to 2-butanone.

Pristine and Postelectrolysis Catalyst Characterization

To better understand the superior performance of PdCu in 1-butene ketonization, we investigated the structural and electronic differences among Pd, PdCu, and HT-PdCu. The chemistry at the catalyst-electrolyte interface is dynamic and differes drastically from the bulk electrolyte under operating conditions.[39−41] For example, the local pH at the catalyst's surface during alkene electro-oxidation could be lower than in the bulk electrolyte as protons accumulate during the generation of reactive oxygen species, which could lead to Cu leaching. However, dissolution may also be associated with catalyst reconstruction that, in some cases, can promote activity.[36,37,42] On the other hand, reconstruction may act as a deactivation pathway, converting active reaction sites into inactive ones.[43] Understanding the changes of pristine catalysts under electrochemical conditions is therefore critical to the future optimization of electrocatalytic systems. Accordingly, we characterized both the pristine and postelectrolysis Pd, PdCu, and HT-PdCu catalysts. The postelectrolysis samples were collected after bulk electrolysis under standard conditions (chronoamperometry at 1.8 V_{RHE} for 30 min in an electrolyte

https://doi.org/10.1021/acscatal.5c08675
ACS Catal. 2026, 16, 7429−7438

of pH 6 with 1-butene). Details on the sample preparation for characterization are provided in SI Section A.4.

X-ray diffraction (XRD) patterns show that pristine PdCu exhibits diffraction peaks closely resembling face-centered cubic (fcc) Pd metal (Figure 3a). Consistent with previous findings on Cu alloying with Pd,[24,44,45] the diffraction peaks of PdCu systematically shift to higher 2θ values due to the incorporation of the smaller Cu atoms into the Pd lattice. Furthermore, the broader peaks for PdCu suggest smaller crystalline domains. The HT-PdCu sample displays a set of diffraction patterns corresponding to a body-centered cubic (bcc) PdO lattice in addition to the fcc Pd which is related to the less oxidized metallic alloy phase (Figure 3a). This suggests that HT-PdCu is partially oxidized, with both oxide and metallic phases present. Both fcc Pd and bcc PdO phases in HT-PdCu shift to higher 2θ values, albeit to a lesser extent than in PdCu, which could point to a lower degree of Cu and Pd alloying due to partial phase segregation during thermal treatment.[46] The sharpness of these peaks can be attributed to larger crystallite sizes of the particle at higher temperatures.[44,47,48] In summary, the XRD analysis revealed that PdCu has a relatively crystalline metallic fcc structure, whereas HT-PdCu contains a mixture of metallic fcc and oxidized bcc phases with larger crystalline domains.

The broadness of the peaks in the XRD spectra hints at the presence of amorphous phases. To examine the nature of the Cu species in PdCu and HT-PdCu, we employed X-ray absorption near-edge spectroscopy (XANES) at the Cu K edge to probe the oxidation states of Cu on both pristine and postelectrolysis samples. Figure 3b shows the XANES spectra of PdCu and HT-PdCu alongside those of standard Cu materials. The absorbance onset of pristine and postelectrolysis PdCu occurs around 8970 eV, within the range of less oxidized Cu species, namely Cu(0) and $Cu(I)_2O$. However, the white line position of PdCu lies close to that of Cu(II) materials, Cu(II)O and $Cu(II)(OH)_2$, indicating a mixture of Cu species with varying valencies. To deconvolute the spectra, linear combination fitting (LCF) was performed using standard spectra. The original and LCF spectra are shown together in Figure 3c. Based on LCF analysis, bulk PdCu likely consists of roughly 20% Cu(0) and 20% Cu(I) species in addition to Cu(II). Given that the XRD pattern of PdCu only detects a metallic fcc phase, the more oxidized Cu phases could have been more amorphous and undetectable by XRD. After electrolysis, the bulk PdCu becomes slightly more oxidized, as Cu(0) is no longer found in the fitting. LCF analysis for pristine and postelectrolysis HT-PdCu indicates predominantly Cu(II) species. However, we were unable to obtain a better fitting for the rising edge region; the fits for the rising edge region were offset by about 3 eV relative to the experimental spectra. This could suggest that HT-PdCu might contain Cu species that are slightly more oxidized than Cu(II) due to the electronic effects of Pd and are not fully captured by the reference standards.

As the surface is the most critical region of the catalyst, we then turned to X-ray photoelectron spectroscopy (XPS) to interrogate the oxidation states of the surface species. Figure 3d,3e shows *ex situ* XPS spectra of Pd, PdCu, and HT-PdCu in both pristine and postelectrolysis states (peak deconvolution is provided in SI Section D.3). The pristine Pd catalyst is predominantly Pd(0), with a Pd $3d_{5/2}$ binding energy at 335.5 eV, and contains approximately 10% Pd(II) at 336.5 eV.[49] Interestingly, the pristine PdCu exhibits a dominant Pd $3d_{5/2}$ peak (Pd(II) shifted) in the range of the binding energy characteristics of Pd(II)[49−51] but with a substantial increase of 1 eV in comparison to the Pd catalyst. This peak is also present in HT-PdCu. Such an energy shift may have resulted from the substitution of smaller Cu^{2+} atoms for larger Pd^{2+} atoms as observed in PdCuO solid solution.[45] It has been suggested that as the lattice contracts due to the substitution, the increase in Madelung energy leads to a higher binding energy.[45] This observation indicates that Cu^{2+} and Pd^{2+} are likely mixed in an oxidized alloy phase at the catalyst surface. In addition, the pristine HT-PdCu contains another component at a binding energy of 338 eV, which can be tentatively assigned as Pd(IV) based on literature reports.[52−54] The formal 4+ oxidation state is known to be unstable for Pd in solution. Although a highly oxidized species could be plausibly stabilized at the surface, such an assignment would require systematic studies. We emphasize that this assignment is tentative and does not imply a true +4 valency; the label "Pd(IV)" is used solely to indicate the tentative assignment. Postelectrolysis spectra are shown as dashed lines in Figure 3d to allow direct comparison with pristine materials. After being subjected to oxidative potential, the Pd catalyst surface becomes significantly oxidized with the emergence of Pd(II) and the "Pd(IV)" components. In contrast, HT-PdCu exhibits less pronounced change after electrolysis, as further oxidation of Pd species in HT-PdCu is unlikely. Most remarkably, in surprising contrast to Pd(II) as the main species in the pristine PdCu, Pd(0) becomes the dominant species in the postelectrolysis PdCu, in addition to the appearance of the Pd(IV) component.

The Cu 2p XPS spectrum of the pristine PdCu (Figure 3e) exhibits a main peak at 933 eV ($2p_{3/2}$) with asymmetry likely arising from a mixture of Cu(0)/Cu(I) at 931 eV and Cu(II) in CuO at 933 eV.[45,55,56] The shakeup features, which stem from valence excitation in paramagnetic states, around 940 and 963 eV are characteristic of Cu(II).[55,56] It should be noted that Cu(0) and Cu(I) are largely indistinguishable in Cu 2p XPS, especially in the presence of a substantial amount of Cu(II).[55] While Cu(I) species are detected in the bulk structure by XAS, we cannot definitively include the presence of Cu(I) at the catalyst surface. After electrolysis, the PdCu surface shows the emergence of a new peak at 934.8 eV, assignable to Cu(II) in $Cu(OH)_2$.[55] In HT-PdCu, Cu is predominantly present as Cu(II), and the $Cu(OH)_2$ peak is also observed on the postelectrolysis surface. Notably, Cu(0)/(I) remains detectable on the PdCu surface after electrolysis. Overall, less oxidized Cu surface species are present in both pristine and postelectrolysis PdCu surfaces, in addition to the emergence of $Cu(OH)_2$ after electrolysis. In contrast, the HT-PdCu surface contains mostly CuO in the pristine state and both CuO and $Cu(OH)_2$ after electrolysis.

As XPS data unveil the formation of new species at the catalyst surfaces after electrolysis, scanning electron microscopy (SEM) was utilized to investigate morphological changes in the catalyst-loaded carbon paper electrodes. SEM images of postelectrolysis PdCu and HT-PdCu electrodes indicate the formation of a nanosheet structure (Figure 3f,g). Nanosheet structures are not observed in pristine PdCu and HT-PdCu, suggesting that these surface features are likely to be induced by the applied potential and the interaction with the electrolyte. Potential-driven reconstruction of Cu oxides to hydroxides has previously been observed, associated with sheet and wire-like growth habits.[57] Elemental mapping constructed from energy-dispersive X-ray spectroscopy (EDS) shows a

https://doi.org/10.1021/acscatal.5c08675
ACS Catal. 2026, 16, 7429−7438

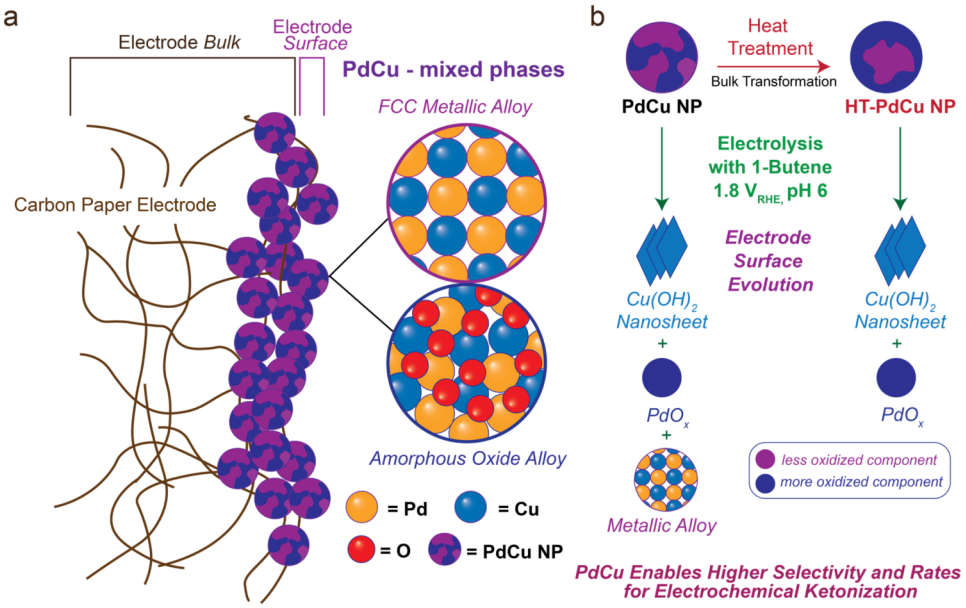

Figure 4. Schematics of catalyst-loaded electrode and surface evolution under operating conditions.

significant phase separation within the nanosheet structure (Figure 3g). The nanosheet primarily consists of Cu and hence is assigned to $Cu(OH)_2$, whereas the Pd signals are concentrated on the nanoparticle clusters. In addition to the nanosheet clusters, the postelectrolysis PdCu retains nanoparticle morphologies (Figure 3f), resembling those of pristine PdCu (Figure S18) and presenting a more uniform Pd and Cu distribution (Figures S20, S22−S25 for HRTEM-EDS). By contrast, the nanoparticle features are not found in the postelectrolysis HT-PdCu.

In summary, bulk- and surface-sensitive characterization techniques reveal that PdCu catalysts contain multiple phases with varying degrees of oxidation (Figure 3). Cu(I) and Cu(II) species are detected in bulk by XAS but are absent in XRD, suggesting that PdCu likely contains amorphous oxide phases along with the fcc metallic alloy phase observed by XRD. The shifted Pd(II) peak in the photoemission spectrum of PdCu indicates the presence of a surface oxide-alloy species in addition to a surface fcc metallic alloy component (Figure 4a). While it is difficult to differentiate Cu(0) and Cu(I) in XPS with a considerable amount of Cu(II),[55] the detection of Pd(0) by XPS in both pristine and postelectrolysis PdCu suggests that Cu(0) is more likely, as it would be energetically favorable to form the PdCu alloy. Moreover, the observation of the shifted metallic fcc phase (Figure S26), rather than pure fcc Pd(0), in the postelectrolysis PdCu by XRD, further supports the presence of the metallic alloy. The absence of the Cu(0) component in the fitted XANES spectrum of the post-electrolysis PdCu (Figure 3c) may be explained by the localization of the less oxidized Cu phase at the catalyst surface, as indicated in the Cu 2p XPS spectrum, rendering it undetectable by XAS. Thermal treatment of the PdCu leads to the mixed-phased HT-PdCu, consisting of the fcc metallic alloy and bcc oxide phases (Figure 4b). As Pd(0) is not observed in XPS, the metallic phase is likely to be concentrated in the bulk rather than at the surface.

Under operating conditions for 1-butene oxidation, the PdCu catalyst exhibits higher selectivity and activity toward 2-butanone formation compared with HT-PdCu. Specifically, ketonization of 1-butene was enhanced 2-fold in selectivity and 4-fold in rate with PdCu (Figure 1a). Considering that the HT-PdCu surface appears more oxidized due to thermal treatment, the improvement in ketonization with PdCu indicates that the native metallic or less oxidized character of the surface PdCu species is likely to play a crucial role in ketone formation, in agreement with previous studies on alkene electro-oxidation with propylene.[11,14] The difference in activity between PdCu and HT-PdCu therefore suggests a catalyst-phase-dependent selectivity between epoxidation and ketonization. Additionally, PdCu shows potential-dependent epoxide-ketone selectivity based on the OER onset potential (Figure 2b,c). Below the OER onset potential, ketonization is favored, while epoxidation overtakes at higher potentials. The observed high ketone selectivity at lower potentials indicates that oxygen intermediates with mild oxidizing ability favor ketone formation. In addition to kinetic competition between oxygen intermediates, it is also plausible that more oxidizing potentials lead to the loss of the less oxidized sites, hence resulting in decreased ketone selectivity. Consequently, the catalyst-phase-dependent selectivity can be compounded by reaction kinetics. Applied potential modulates the electronic properties and thermodynamics of the catalyst surface species, altering the reactivity of oxygen intermediates and thereby affecting ketone-epoxide selectivity. Therefore, ketone-epoxide selectivity can be influenced by both catalyst phase change and external potential, with potential-induced surface changes further complicating the factors governing selectivity.

Postelectrolysis characterization of catalyst-loaded electrodes provides insight into the potential-induced surface changes. Formation of $Cu(OH)_2$ was observed via XPS and SEM on the surfaces of PdCu- and HT-PdCu-loaded electrodes after electrolysis (Figure 3e,g). Considering the poor ketonization performance by HT-PdCu, $Cu(OH)_2$ is unlikely to account for the superior performance of PdCu. Moreover, surface "Pd(IV)" species were detected on all three postelectrolysis electrode surfaces, suggesting oxidation of the surface Pd species under operating conditions (Figure 3d). Intriguingly, not all of the Pd species on the PdCu surface become more

https://doi.org/10.1021/acscatal.5c08675
ACS Catal. 2026, 16, 7429−7438

oxidized under anodic polarization. Although the surface Pd(II) species was observed as the dominant species in pristine PdCu, Pd(0) becomes the main component after electrolysis. Moreover, the surface Cu species in PdCu did not fully convert to Cu(II), even under the same electrochemical conditions that oxidize the majority of Pd(0) in monometallic Pd. Uniform Pd and Cu elemental mapping on the postelectrolysis PdCu electrode indicates a high degree of Pd−Cu mixing within the nanoparticle structures (Figure S20). These spectroscopic observations point to a metallic alloy component on the PdCu surface after electrolysis, in contrast with the predominantly oxidized surfaces of metallic Pd and HT-PdCu. The superior ketonization performance of PdCu thus may arise not only from its metallic surface species in the pristine state but also from its ability to retain the metallic phase under anodic polarization. This unusual resistance to surface oxidation is likely a result of the electronic effects of alloying Pd and Cu.

CONCLUSIONS

This work expands the scope of alkene electro-oxidation by reporting the heterogeneous ketonization of 1-butene to 2-butanone using a bimetallic PdCu electrocatalyst in aqueous electrolytes. While previous research has largely focused on propylene epoxidation, we present the first study of electro-oxidation of 1-butene, which is inherently more challenging due to poorer aqueous solubility and reactivity caused by the longer carbon chain. We demonstrated selective generation of 2-butanone for its industrial relevance and promising status as a fossil fuel alternative. We established the heterogeneous nature of the system and showed that the PdCu catalyst achieves a 4-fold enhancement in product rate and a 2-fold improvement in Faradaic efficiency for 2-butanone compared to monometallic Pd and preoxidized controls. Notably, ketone-epoxide selectivity can be modulated by the applied potential, with ketonization favored below the OER onset potential. Furthermore, 2-butanone generation exhibits a weak dependence on both applied potentials and bulk electrolyte pHs, suggesting that the reaction is likely limited by a thermochemical rather than an electrochemical step. Characterization of pristine and postelectrolysis electrodes revealed that alloying Pd and Cu generates a metallic phase that remains largely preserved under anodic polarization, in contrast to the monometallic Pd control and the preoxidized analogue. We propose that this metallic phase is responsible for the improved ketonization activity. Collectively, these findings indicate that the metallic PdCu phase drives the selective ketonization of 1-butene, offering a framework for the rational design of future alkene ketonization electrocatalysts.

METHODS

Catalyst and Electrode Preparation

The bimetallic PdCu catalyst was synthesized via a coreduction method that was adapted from a literature procedure.[24] Briefly, 0.25 mmol of palladium(II) chloride (Thermo Scientific, 99%) and 0.25 mmol of copper(II) chloride (Acros Organis, 99%) solutions were combined with 1.25 mmol of trimethyl(tetradecyl)ammonium bromide (Sigma-Aldrich, 99%) in 200 mL Milli-Q water. The solutions were cooled below 10 °C. Six mmol of L-ascorbic acid (Sigma-Aldrich, Reagent grade) was then added. The reaction mixture was kept cool and stirred rigorously overnight. The product was washed with abundant Milli-Q water and collected and dried at 60 °C overnight under vacuum. The catalyst powder, reddish brown in color, was collected and ground with a mortar and pestle so that the catalyst powder had a consistent and fine texture. The powder was stored at room temperature. The pure Pd material was synthesized following the same procedure with 0.5 mmol of palladium(II) chloride with no addition of copper(II) chloride.

PdCu-loaded electrodes were prepared by drop-casting catalyst ink solutions [5 mg of PdCu powder and 2 mg of carbon black (Vulcan XC 72, Fuel Cell Store) in 1 mL of water/IPA (1:4 w/w)] onto a Sigracet carbon paper (Sigracet 39 BB, 5 wt % PTFE, Fuel Cell Store). A total of 300 μL of catalyst ink was drop-casted in 50 μL increments. Electrodes were then coated with 50 μL of 2 wt % Nafion solution and dried at 80 °C overnight.

Electrolyte Preparation

Aqueous electrolyte solutions were used in the electrochemical studies. All electrolyte formulations used 0.9 M sodium perchlorate (Sigma-Aldrich, 98%), and the bulk pH was controlled via the 0.25 M sodium phosphate buffer. The electrolytes were prepared from 5 M $NaClO_4$ and 1/0.5 M sodium phosphate stock solutions. The buffer solutions were prepared by dissolving the theoretically determined amount of phosphoric acid (Mallinckrodt 85%), sodium phosphate monobasic (Sigma-Aldrich, 98%), sodium phosphate dibasic heptahydrate (Acros Organis, 99+%), and sodium phosphate (Sigma-Aldrich, 96%) in Milli-Q water and adjusting to the desired pH value with 1 M NaOH and 1 M H_3PO_4 solutions.

Electrochemical Reaction Setup and Product Quantification

Electrochemical experiments were performed in a sandwich-style electrochemical cell in a gas-diffusion configuration with a piece of platinum foil (Beantown Chemical, 99.99%) as the counter electrode and catalyst-loaded carbon paper as the working electrode. A leakless Ag/AgCl electrode (eDAQ) was used as the reference electrode. Aluminum foils (Reynold's Wrap) acted as the current collectors for both the anode and cathode. Hydrophobic carbon paper (Toray Carbon Paper 120, 5% wet-proofed, Fuel Cell Store) was placed behind the catalyst-loaded carbon paper to prevent electrolyte flooding. The total volume of the electrolyte is 3.6 mL, and an ambient flow of 1-butene was introduced to the cell in a pass-through configuration during the bulk electrolysis.

The electrochemical measurements were conducted with a BioLogic VMP3Multichannel potentiostat. The solution resistance was measured at open circuit potential (OCP) by electrochemical impedance spectroscopy techniques from 200 kHz to 100 mHz at 10 mV amplitude, and the resulting resistance determined from the x-intercept in the Nyquist plot was input for 100% *iR* compensation. The electrolysis experiments were conducted at fixed applied potentials for 30 min.

The postelectrolysis electrolytes were collected and dispensed into a 5 mL volumetric flask. The electrolyte chamber was rinsed with additional Milli-Q water, which was then transferred to the volumetric flask until the total volume reached the mark. 540 μL of the electrolyte was added to a clean NMR tube in addition to 60 μL of the internal standard solution, ∼1 mM 3-(Trimethylsilyl)-1-propanesulfonic acid sodium salt (Fluka Chemika, 99%) in D_2O. The products were quantified using ^{1}H NMR spectroscopy. The NMR spectra were acquired on a Bruker 400 MHz spectrometer with water suppression performed. The 1H probe was automatically tuned, and the solvent lock was done with 90% H_2O and 10% D_2O, and gradient shimming and autogain were used. 32 scans were collected per sample, and relaxation delay was set at 3 s.

Powder XRD Analysis

The X-ray diffraction patterns of the synthesized catalysts were obtained using an X-ray powder diffractometer (Rigaku SmartLab) with Cu Kα radiation (λ = 1.54056 Å). The diffraction patterns were collected from 10 to 90° 2θ at a step size of 0.01° and 5° per minute. Data were processed by using HighScore software.

https://doi.org/10.1021/acscatal.5c08675
ACS Catal. 2026, 16, 7429−7438

X-ray Photoelectron Spectroscopy

XPS measurements were collected using an AXIS Nova spectrometer by Analytical and analyzed with CasaXPS software. XPS samples were prepared by pressing the sample powders and standard materials into a 3 mm diameter pellet. After electrolysis, the electrodes were rinsed with Milli-Q water and dried under vacuum in a vacuum desiccator. The samples were directly attached to the sample platen with the platen's clips. The carbon 1s spectrum was always acquired for all of the measurements so that the adventitious carbon at 285 eV could be used to calibrate the charging effect.

X-ray Absorption Spectroscopy

All XAS measurements were collected with an easyXAFS300 spectrometer in transmission mode with X-ray operating at 40 kV and 25 mA. The standard materials and catalyst powders were diluted with sucrose to ca. 10% and 15−18%, respectively, and homogenized with a mortar and pestle. The resulting mixture was pressed into a 3 mm diameter pellet and sealed with Kapton. The postelectrolysis spectra were obtained by pressing the spent catalyst-loaded carbon paper electrodes into a 3 mm diameter pellet to increase the volumetric concentration. A standard XAS Cu foil was used to calibrate the energy shift. The raw spectra were analyzed and processed via the ATHENA suite to obtain normalized spectra. The linear combination fitting function in ATHENA was used to fit the spectra of the standard samples to those of the catalysts.

Scanning Electron Microscopy and High-Resolution Transmission Electron Microscopy

The morphologies of the pristine and postelectrolysis electrodes were collected with a ZEISS 15,500VP field-emission scanning electron microscope equipped with an Oxford X-MAS SDD EDS system. Catalyst-loaded carbon paper electrodes and vacuum-dried post-electrolysis carbon paper were attached to the SEM holders with carbon tape; extra copper tape was used to ground the sample. A turbo carbon evaporator was used to coat the sample with a thin layer of carbon (<10 nm). All TEM characterizations were performed using an FEI Titan 80−300 scanning transmission electron microscope operated at 300 kV equipped with a field-emission gun, Oxford X-MaxN 100TLE 100 mm^2 SDD X-ray spectrometer, and a Gatan Ultrascan digital camera. A small amount of diluted PdCu catalyst ink was drop-casted onto the TEM grid. The postelectrolysis PdCu-loaded carbon paper was sonicated with a probe sonicator in IPA to extract the catalyst powder. The resulting homogeneous solution was drop-casted onto the TEM grid. The sample-loaded TME grids were allowed to air-dry.

■ ASSOCIATED CONTENT

Supporting Information

The Supporting Information is available free of charge at https://pubs.acs.org/doi/10.1021/acscatal.5c08675.

Experimental methods, including materials, catalyst and electrode preparation, electrochemical experiments, and product analysis; additional data of catalyst characterization and discussions (PDF)

■ AUTHOR INFORMATION

Corresponding Author

Karthish Manthiram − *Division of Chemistry and Chemical Engineering, California Institute of Technology, Pasadena, California 91125, United States;* orcid.org/0000-0001-9260-3391; Email: karthish@caltech.edu

Authors

Chenyu Jiang − *Division of Chemistry and Chemical Engineering, California Institute of Technology, Pasadena, California 91125, United States*

Benjamin Moss − *Division of Chemistry and Chemical Engineering, California Institute of Technology, Pasadena, California 91125, United States*

Alexis Lindenfelser − *Division of Chemistry and Chemical Engineering, California Institute of Technology, Pasadena, California 91125, United States*

Jung Tae Kim − *Department of Chemical and Biomolecular Engineering, University of California, Los Angeles, California 90095, United States*

Yuzhang Li − *Department of Chemical and Biomolecular Engineering, University of California, Los Angeles, California 90095, United States;* orcid.org/0000-0002-1502-7869

Complete contact information is available at: https://pubs.acs.org/10.1021/acscatal.5c08675

Notes

The authors declare no competing financial interest.

■ ACKNOWLEDGMENTS

The catalyst design, catalyst synthesis, kinetic studies, and XRD, XPS, XAS, and SEM-EDX characterization were supported by the Liquid Sunlight Alliance, which is funded by the U.S. Department of Energy, Office of Science, Office of Basic Energy Sciences, Fuels from Sunlight Hub under Award Number DE-SC0021266. We acknowledge the support of the Resnick Sustainability Institute for providing the easyXAFS spectrometer. We thank Channing Klein, Thu Ton, Kalipada Koner, Emma Cosner, Spencer Delgado-Kukuczk, Michael Yusov, and Evan Miu for insightful discussions and help. Y.L. acknowledges research support for electron microscopy characterization from the Department of Energy, Office of Basic Energy Sciences, Electron and Scanning Probe Microscopies Program under award DE-SC0022955 and the Camille Dreyfus Teacher Scholar Award (TC-25-036).

■ REFERENCES

(1) Segovia-Hernández, J. G.; Núñez-López, J. M.; Cossío-Vargas, E.; Juárez-García, M.; Sánchez-Ramírez, E. Electrification in the Chemical Industry and Its Role in Achieving Carbon Neutrality: Areas, Challenges, and Opportunities for Process Intensification. *RSC Sustainable* **2025**, *3* (11), 4955−4974.

(2) Ali, S. A.; Bangash, I. A.; Sajjad, H.; Karim, M. A.; Ahmad, F.; Ahmad, M.; Habib, K.; Shah, S. N.; Sami, A.; Laghari, Z. A.; Qudoos, A. Review on the Role of Electrofuels in Decarbonizing Hard-to-Abate Transportation Sectors: Advances, Challenges, and Future Directions. *Energy Fuels* **2025**, *39* (11), 5051−5098.

(3) Methyl Ethyl Ketone (MEK) Market Size to Reach USD 5.3 Bn 2034 https://www.towardschemandmaterials.com/insights/methyl-ethyl-ketone-market. (accessed October 26, 2025).

(4) Ackermann, P.; Braun, K. E.; Burkardt, P.; Heger, S.; König, A.; Morsch, P.; Lehrheuer, B.; Surger, M.; Völker, S.; Blank, L. M.; et al. Designed to Be Green, Economic, and Efficient: A Ketone-Ester-Alcohol-Alkane Blend for Future Spark-Ignition Engines. *ChemSusChem* **2021**, *14* (23), 5254−5264.

(5) Torres-Vinces, L.; Contreras-Zarazua, G.; Huerta-Rosas, B.; Sánchez-Ramírez, E.; Segovia-Hernández, J. G. Methyl Ethyl Ketone Production through an Intensified Process. *Chem. Eng. Technol.* **2020**, *43* (7), 1433−1441.

(6) Sun, Y.; Hu, H.; Li, Y. Electro-Oxidation of Alkenes: A Green Approach Towards Functionalized Oxygenates. *ChemCatChem* **2024**, *16* (13), No. e202301534.

(7) Jin, K.; Maalouf, J. H.; Lazouski, N.; Corbin, N.; Yang, D.; Manthiram, K. Epoxidation of Cyclooctene Using Water as the Oxygen Atom Source at Manganese Oxide Electrocatalysts. *J. Am. Chem. Soc.* **2019**, *141* (15), 6413−6418.

(8) Chung, M.; Jin, K.; Zeng, J. S.; Ton, T. N.; Manthiram, K. Tuning Single-Atom Dopants on Manganese Oxide for Selective Electrocatalytic Cyclooctene Epoxidation. *J. Am. Chem. Soc.* **2022**, *144* (38), 17416−17422.
(9) Chung, M.; Maalouf, J. H.; Adams, J. S.; Jiang, C.; Román-Leshkov, Y.; Manthiram, K. Direct Propylene Epoxidation via Water Activation over Pd-Pt Electrocatalysts. *Science* **2024**, *383* (6678), 49−55.
(10) Koroidov, S.; Winiwarter, A.; Diaz-Morales, O.; Görlin, M.; Stenlid, J. H.; Wang, H.-Y.; Börner, M.; Goodwin, C. M.; Soldemo, M.; Pettersson, L. G. M.; et al. Chemisorbed Oxygen or Surface Oxides Steer the Selectivity in Pd Electrocatalytic Propene Oxidation Observed by *Operando* Pd L-Edge X-Ray Absorption Spectroscopy. *Catal. Sci. Technol.* **2021**, *11* (10), 3347−3352.
(11) Liu, X.-C.; Wang, T.; Zhang, Z.-M.; Yang, C.-H.; Li, L.-Y.; Wu, S.; Xie, S.; Fu, G.; Zhou, Z.-Y.; Sun, S.-G. Reaction Mechanism and Selectivity Tuning of Propene Oxidation at the Electrochemical Interface. *J. Am. Chem. Soc.* **2022**, *144* (45), 20895−20902.
(12) Winiwarter, A.; Silvioli, L.; B Scott, S.; Enemark-Rasmussen, K.; Sariç, M.; B Trimarco, D.; K Vesborg, P. C.; G Moses, P.; L Stephens, I. E.; Seger, B.; et al. Towards an Atomistic Understanding of Electrocatalytic Partial Hydrocarbon Oxidation: Propene on Palladium. *Energy Environ. Sci.* **2019**, *12* (3), 1055−1067.
(13) Huang, J. E.; Chen, Y.; Ou, P.; Ding, X.; Yan, Y.; Dorakhan, R.; Lum, Y.; Li, X.-Y.; Bai, Y.; Wu, C.; et al. Selective Electrified Propylene-to-Propylene Glycol Oxidation on Activated Rh-Doped Pd. *J. Am. Chem. Soc.* **2024**, *146* (12), 8641−8649.
(14) Li, D.; Sun, P.; Zhang, D.; Li, H.; Xu, H.; Cao, D. Unraveling the Potential-Dependent Selectivity of Propylene Electrooxidation: The Role of Electrochemistry-Induced Reconstruction. *J. Am. Chem. Soc.* **2025**, *147* (28), 24900−24912.
(15) Yun, T. G.; Chen, B.; Wells, S.; Lim, Y.; Kim, J. S.; Buzanich, A. G.; Radtke, M.; Waegele, M. M.; Risch, M.; Grimaud, A. Extrinsic and Intrinsic Factors Governing the Electrochemical Oxidation of Propylene in Aqueous Solutions. *J. Am. Chem. Soc.* **2025**, *147* (14), 12318−12330.
(16) Iguchi, S.; Kataoka, M.; Hoshino, R.; Yamanaka, I. Direct Epoxidation of Propylene with Water at a PtOx Anode Using a Solid-Polymer-Electrolyte Electrolysis Cell. *Catal. Sci. Technol.* **2022**, *12* (2), 469−473.
(17) Ke, J.; Zhao, J.; Chi, M.; Wang, M.; Kong, X.; Chang, Q.; Zhou, W.; Long, C.; Zeng, J.; Geng, Z. Facet-Dependent Electrooxidation of Propylene into Propylene Oxide over Ag3PO4 Crystals. *Nat. Commun.* **2022**, *13* (1), No. 932.
(18) Tsuji, J. Synthetic Applications of the Palladium-Catalyzed Oxidation of Olefins to Ketones. *Synthesis* **1984**, *1984*, 369−384.
(19) Keith, J. A.; Henry, P. M. The Mechanism of the Wacker Reaction: A Tale of Two Hydroxypalladations. *Angew. Chem., Int. Ed.* **2009**, *48*, 9038−9049.
(20) Espeel, P. H.; Tielen, M. C.; Jacobs, P. A. Palladium−Copper-Exchanged Y Type Zeolites: A True Heterogeneous Wacker Catalyst. *J. Chem. Soc. Chem. Commun.* **1991**, *49* (10), 669−671.
(21) Imbao, J.; van Bokhoven, J. A.; Clark, A.; Nachtegaal, M. Elucidating the Mechanism of Heterogeneous Wacker Oxidation over Pd-Cu/Zeolite Y by Transient XAS. *Nat. Commun.* **2020**, *11* (1), No. 1118.
(22) Imbao, J.; van Bokhoven, J. A.; Nachtegaal, M. On the Promotional and Inhibitory Effects of Water on Wacker-Type Ethylene Oxidation Over Pd−Cu/Zeolite Y. *ACS Catal.* **2021**, *11* (14), 8684−8691.
(23) Kumar, A.; Deka, S. Focused Review on the Use of Bimetallic Alloy Nanoparticle Electrocatalysts in Water Splitting Reactions. *J. Phys. Chem. C* **2024**, *128* (45), 19037−19054.
(24) Zhou, R.; Fan, X.; Ke, X.; Xu, J.; Zhao, X.; Jia, L.; Pan, B.; Han, N.; Li, L.; Liu, X.; et al. Two-Dimensional Palladium−Copper Alloy Nanodendrites for Highly Stable and Selective Electrochemical Formate Production. *Nano Lett.* **2021**, *21* (9), 4092−4098.
(25) Xiong, Y.; Ye, W.; Chen, W.; Wu, Y.; Xu, Q.; Yan, Y.; Zhang, H.; Wu, J.; Yang, D. PdCu Alloy Nanodendrites with Tunable Composition as Highly Active Electrocatalysts for Methanol Oxidation. *RSC Adv.* **2017**, *7* (10), 5800−5806.
(26) Pei, G. X.; Liu, X. Y.; Yang, X.; Zhang, L.; Wang, A.; Li, L.; Wang, H.; Wang, X.; Zhang, T. Performance of Cu-Alloyed Pd Single-Atom Catalyst for Semihydrogenation of Acetylene under Simulated Front-End Conditions. *ACS Catal.* **2017**, *7* (2), 1491−1500.
(27) Ma, M.; Zhu, W.; Shao, Q.; Shi, H.; Liao, F.; Shao, C.; Shao, M. Palladium−Copper Bimetallic Nanoparticles Loaded on Carbon Black for Oxygen Reduction and Zinc−Air Batteries. *ACS Appl. Nano Mater.* **2021**, *4* (2), 1478−1484.
(28) Mao, Z.; Xie, Z.; Chen, J. G. Comparison of Heterogeneous Hydroformylation of Ethylene and Propylene over RhCo3/MCM-41 Catalysts. *ACS Catal.* **2021**, *11* (23), 14575−14585.
(29) Porter, W. N.; Lin, Z.; Chen, J. G. Experimental and Theoretical Studies of Reaction Pathways of Direct Propylene Epoxidation on Model Catalyst Surfaces. *Surf. Sci. Rep.* **2021**, *76* (2), No. 100524.
(30) Roithová, J.; Schröder, D. Gas-Phase Models for Catalysis: Alkane Activation and Olefin Epoxidation by the Triatomic Cation Ag2O+. *J. Am. Chem. Soc.* **2007**, *129* (49), 15311−15318.
(31) Nijhuis, T. A.; Makkee, M.; Moulijn, J. A.; Weckhuysen, B. M. The Production of Propene Oxide: Catalytic Processes and Recent Developments. *Ind. Eng. Chem. Res.* **2006**, *45* (10), 3447−3459.
(32) Wang, Y.; Xu, M.; Wang, X.; Ge, R.; Zhu, Y.-Q.; Li, A.-Z.; Zhou, H.; Chen, F.; Zheng, L.; Duan, H. Unraveling the Potential-Dependent Structure Evolution in CuO for Electrocatalytic Biomass Valorization. *Sci. Bull.* **2023**, *68* (23), 2982−2992.
(33) Chen, S.; Farzinpour, F.; Kornienko, N. Dynamic Active Sites behind Cu-Based Electrocatalysts: Original or Restructuring-Induced Catalytic Activity. *Chem* **2025**, *11* (8), No. 102575.
(34) Takamatsu, D.; Fukatani, N.; Yoneyama, A.; Hirano, T.; Hirai, K.; Yabuuchi, S.; Watanabe, K.; Kamiya, K.; Nakanishi, S. Dynamic Relocation of Copper Catalysts in Gas Diffusion Electrodes during CO2 Electroreduction. *J. Am. Chem. Soc.* **2025**, *147* (27), 24103−24112.
(35) Wang, J. Controlling Dynamic Reconstruction Chemistry for Superior Oxygen-Evolving Catalysts. *Chem* **2023**, *9* (7), 1645−1657.
(36) Duan, Y.; Lee, J. Y.; Xi, S.; Sun, Y.; Ge, J.; Ong, S. J. H.; Chen, Y.; Dou, S.; Meng, F.; Diao, C.; et al. Anodic Oxidation Enabled Cation Leaching for Promoting Surface Reconstruction in Water Oxidation. *Angew. Chem., Int. Ed.* **2021**, *60* (13), 7418−7425.
(37) Chung, D. Y.; Lopes, P. P.; Martins, P. F. B.; He, H.; Kawaguchi, T.; Zapol, P.; You, H.; Tripkovic, D.; Strmcnik, D.; Zhu, Y.; et al. Dynamic Stability of Active Sites in Hydr(Oxy)Oxides for the Oxygen Evolution Reaction. *Nat. Energy* **2020**, *5* (3), 222−230.
(38) Zeng, J. S.; Cosner, E. L.; Delgado-Kukuczka, S. P.; Jiang, C.; Adams, J. S.; Román-Leshkov, Y.; Manthiram, K. Electrifying Hydroformylation Catalysts Exposes Voltage-Driven C−C Bond Formation. *J. Am. Chem. Soc.* **2024**, *146* (24), 16521−16530.
(39) Zhang, R.; Pearce, P. E.; Duan, Y.; Dubouis, N.; Marchandier, T.; Grimaud, A. Importance of Water Structure and Catalyst−Electrolyte Interface on the Design of Water Splitting Catalysts. *Chem. Mater.* **2019**, *31* (20), 8248−8259.
(40) Li, G.-F.; Divinagracia, M.; Labata, M. F.; Ocon, J. D.; Chuang, P.-Y. A. Electrolyte-Dependent Oxygen Evolution Reactions in Alkaline Media: Electrical Double Layer and Interfacial Interactions. *ACS Appl. Mater. Interfaces* **2019**, *11* (37), 33748−33758.
(41) Liang, C.; Katayama, Y.; Tao, Y.; Morinaga, A.; Moss, B.; Celorrio, V.; Ryan, M.; Stephens, I. E. L.; Durrant, J. R.; Rao, R. R. Role of Electrolyte pH on Water Oxidation for Iridium Oxides. *J. Am. Chem. Soc.* **2024**, *146* (13), 8928−8938.
(42) Li, S.; Ma, P.; Gao, C.; Liu, L.; Wang, X.; Shakouri, M.; Chernikov, R.; Wang, K.; Liu, D.; Ma, R.; Wang, J. Reconstruction-Induced NiCu-Based Catalysts towards Paired Electrochemical Refining. *Energy Environ. Sci.* **2022**, *15* (7), 3004−3014.
(43) Spöri, C.; Kwan, J. T. H.; Bonakdarpour, A.; Wilkinson, D. P.; Strasser, P. The Stability Challenges of Oxygen Evolving Catalysts: Towards a Common Fundamental Understanding and Mitigation of

https://doi.org/10.1021/acscatal.5c08675
ACS Catal. 2026, 16, 7429−7438

Catalyst Degradation. *Angew. Chem., Int. Ed.* **2017**, *56* (22), 5994−6021.
(44) Kariuki, N. N.; Wang, X.; Mawdsley, J. R.; Ferrandon, M. S.; Niyogi, S. G.; Vaughey, J. T.; Myers, D. J. Colloidal Synthesis and Characterization of Carbon-Supported Pd−Cu Nanoparticle Oxygen Reduction Electrocatalysts. *Chem. Mater.* **2010**, *22* (14), 4144−4152.
(45) Christensen, G. L.; Langell, M. A. Characterization of Copper Palladium Oxide Solid Solutions by X-Ray Diffraction, X-Ray Photoelectron Spectroscopy, and Auger Electron Spectroscopy. *J. Phys. Chem. C* **2013**, *117* (14), 7039−7049.
(46) Jiang, Y.; Lim, A. M. H.; Yan, H.; Zeng, H. C.; Mirsaidov, U. Phase Segregation in PdCu Alloy Nanoparticles During CO Oxidation Reaction at Atmospheric Pressure. *Adv. Sci.* **2023**, *10* (25), No. 2302663.
(47) Wang, C.; Chen, D. P.; Sang, X.; Unocic, R. R.; Skrabalak, S. E. Size-Dependent Disorder−Order Transformation in the Synthesis of Monodisperse Intermetallic PdCu Nanocatalysts. *ACS Nano* **2016**, *10* (6), 6345−6353.
(48) Friedrich, M.; Armbrüster, M. Crystallite Size Controls the Crystal Structure of Cu_{60} Pd_{40} Nanoparticles. *Chem. Mater.* **2009**, *21* (24), 5886−5891.
(49) Brun, M.; Berthet, A.; Bertolini, J. C. XPS, AES and Auger Parameter of Pd and PdO. *J. Electron Spectrosc. Relat. Phenom.* **1999**, *104* (1−3), 55−60.
(50) Peuckert, M. XPS Study on Surface and Bulk Palladium Oxide, Its Thermal Stability, and a Comparison with Other Noble Metal Oxides. *J. Phys. Chem. A* **1985**, *89* (12), 2481−2486.
(51) Jeong, B.; Lee, D.; Park, J.-I.; Lee, S. M. Near Ambient Pressure XPS Investigation of Hydrous Palladium Oxide under Water and Oxygen Gas Environments. *J. Phys. Appl. Phys.* **2021**, *54* (32), No. 324001.
(52) Oh, S.-H.; Hoflund, G. B. Chemical State Study of Palladium Powder and Ceria-Supported Palladium during Low-Temperature CO Oxidation. *J. Phys. Chem. A* **2006**, *110* (24), 7609−7613.
(53) Lupan, O.; Postica, V.; Hoppe, M.; Wolff, N.; Polonskyi, O.; Pauporté, T.; Viana, B.; Majérus, O.; Kienle, L.; Faupel, F.; Adelung, R. PdO/PdO_2 Functionalized ZnO: Pd Films for Lower Operating Temperature H_2 Gas Sensing. *Nanoscale* **2018**, *10* (29), 14107−14127.
(54) Li, Y.; Yu, Y.; Wang, J.-G.; Song, J.; Li, Q.; Dong, M.; Liu, C.-J. CO Oxidation over Graphene Supported Palladium Catalyst. *Appl. Catal. B Environ.* **2012**, *125*, 189−196.
(55) Biesinger, M. C.; Lau, L. W. M.; Gerson, A. R.; Smart, R. St. C. Resolving Surface Chemical States in XPS Analysis of First Row Transition Metals, Oxides and Hydroxides: Sc, Ti, V, Cu and Zn. *Appl. Surf. Sci.* **2010**, *257* (3), 887−898.
(56) Biesinger, M. C. Advanced Analysis of Copper X-Ray Photoelectron Spectra. *Surf. Interface Anal.* **2017**, *49* (13), 1325−1334.
(57) Bai, J.; Wang, Q.; Yang, Z.; Yu, H.; Yang, L.; Zhu, J. The Influence of Reconstructive Transformation from Micro-/Nano-structured Copper(II) Hydroxide to Copper Oxides as Electrodes for High-Performance Supercapacitors. *J. Alloys Compd.* **2024**, *976*, No. 173095.

https://doi.org/10.1021/acscatal.5c08675
ACS Catal. 2026, 16, 7429−7438